RPA in quantum dots

PHYSICAL REVIEW B 68, 035341 (2003)

Symmetry breaking and the random-phase approximation in small quantum dots

Llorenç Serra,[1] Rashid G. Nazmitdinov,[1,2] and Antonio Puente[1]
[1]*Departament de Física, Universitat de les Illes Balears, E-07122 Palma de Mallorca, Spain*
[2]*Bogoliubov Laboratory of Theoretical Physics, Joint Institute for Nuclear Research, 141980 Dubna, Russia*
(Received 10 April 2003; published 31 July 2003)

The random-phase approximation has been used to compute the properties of parabolic two-dimensional quantum dots beyond the mean-field approximation. Special emphasis is put on the ground state correlation energy, the symmetry restoration, and the role of the spurious modes within the random-phase approximation. A systematics with the Coulombic interaction strength is presented for the 2-electron dot, while for the 6- and 12 electron dots selected cases are discussed. The validity of the random phase approximation is assessed by comparison with available exact results.

Summary:

- Introduction
- HF mean field
  - results
- RPA excitations
  - Formalism
  - Spurious modes
  - results
- Strength functions and sum rules
- RPA ground state
  - Symmetry restoration
- Conclusions

Introduction SEMICONDUCTOR QUANTUM DOTS

electron islands with quantized motion

etching process

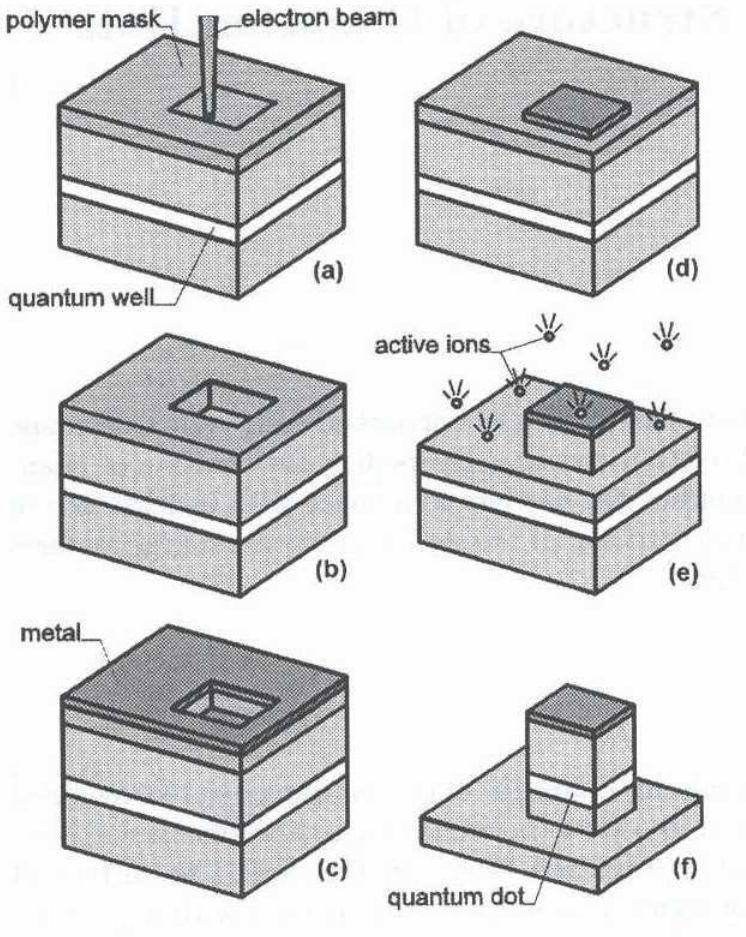

microelectrodes

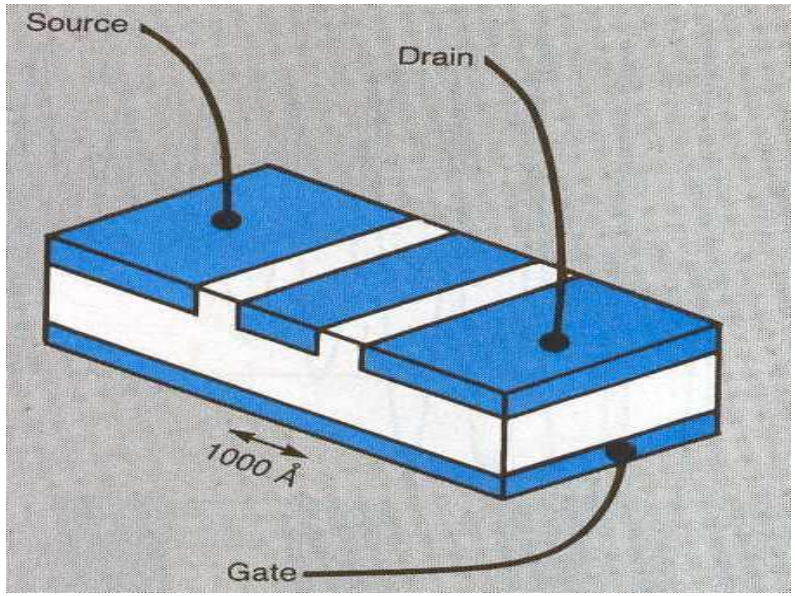

artificial atoms with contacts

Discrete energy levels:

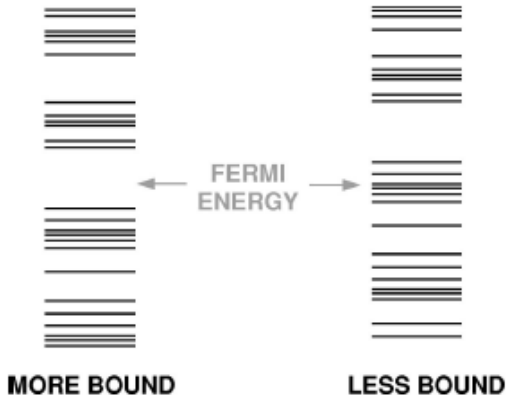

Variation with deformation

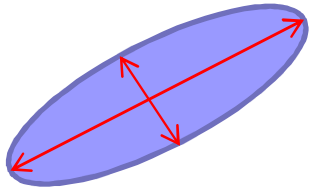

$$\delta = \frac{\omega_x}{\omega_y}$$

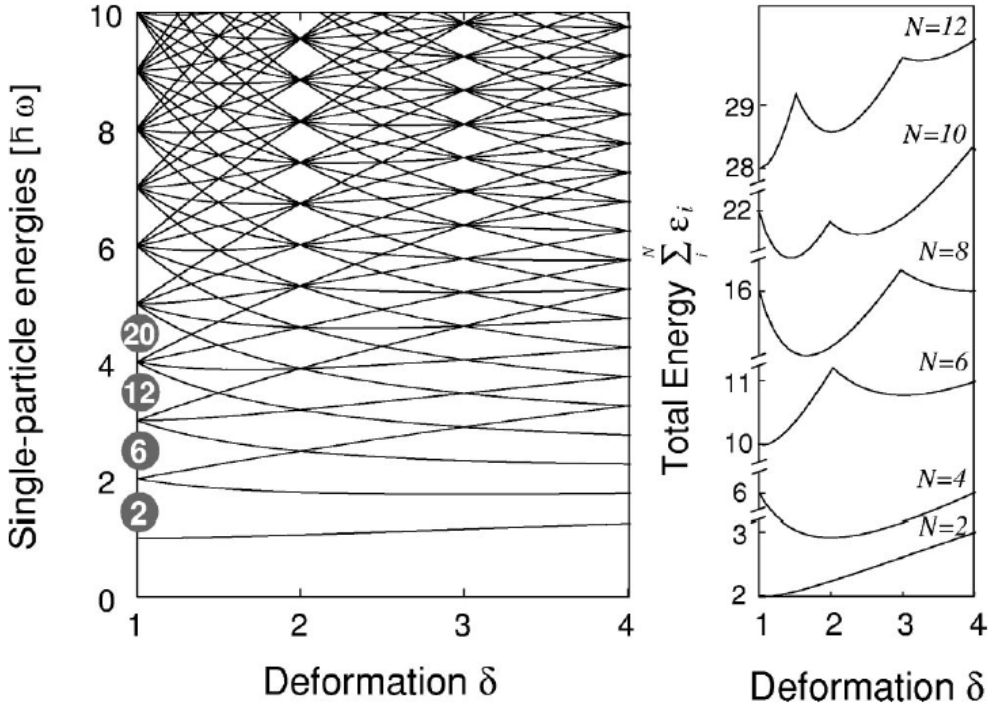

SHELL STRUCTURE (another case)

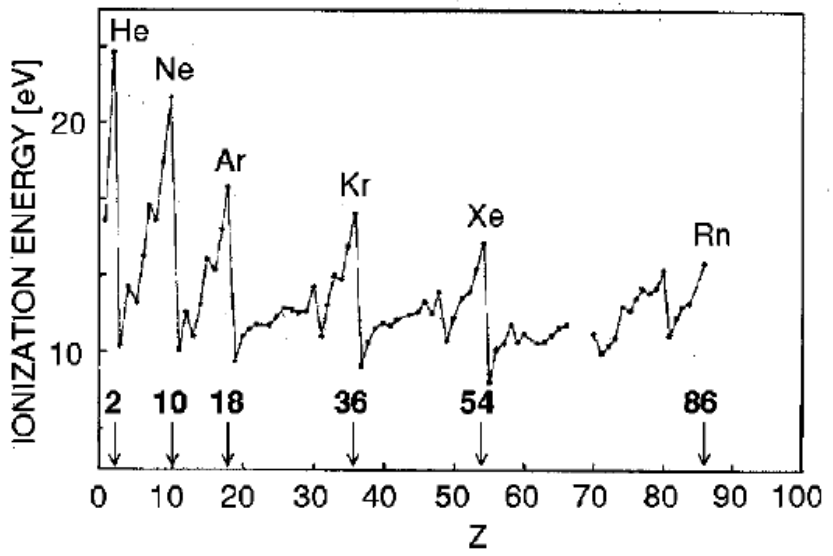

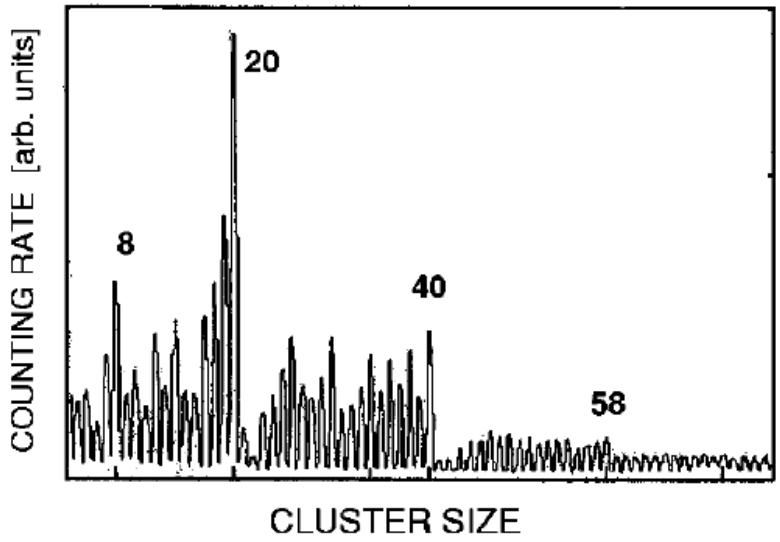

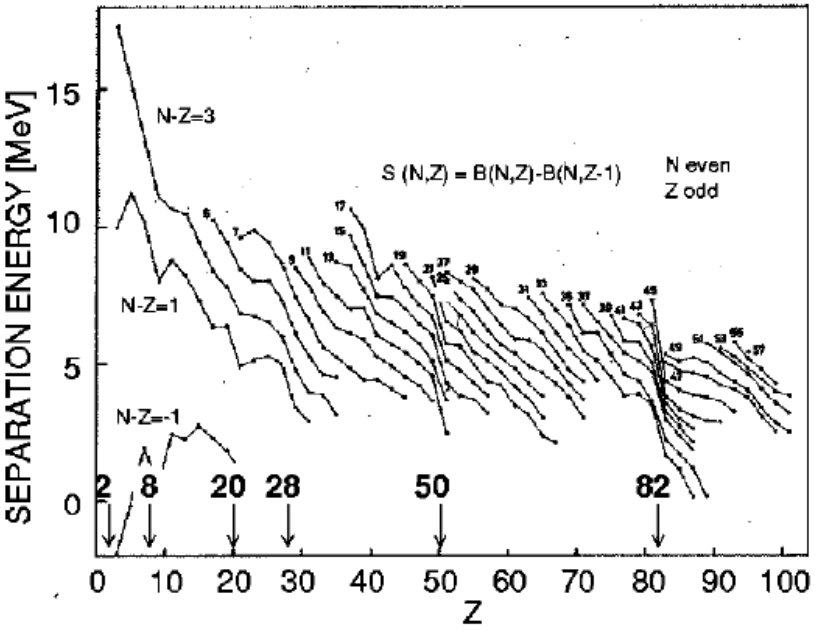

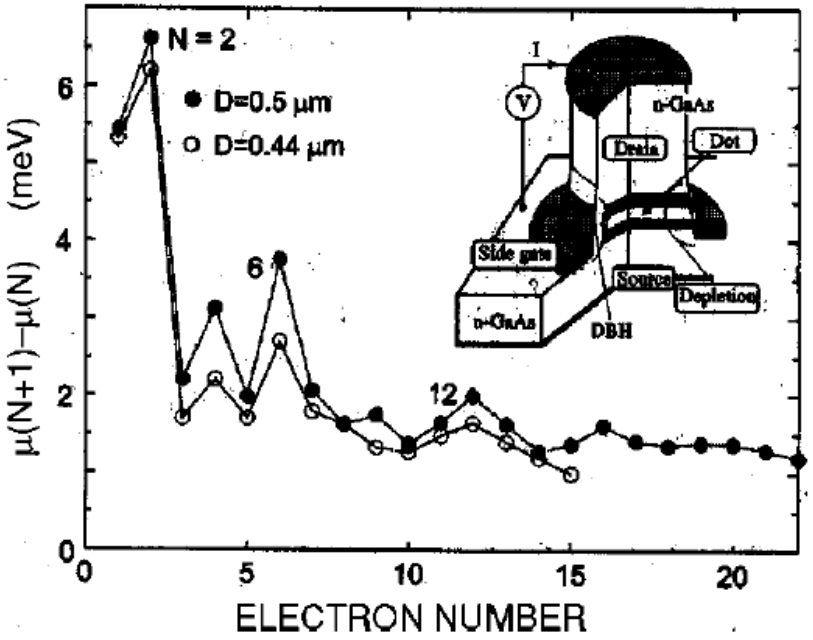

1 Vertical quantum dot structure

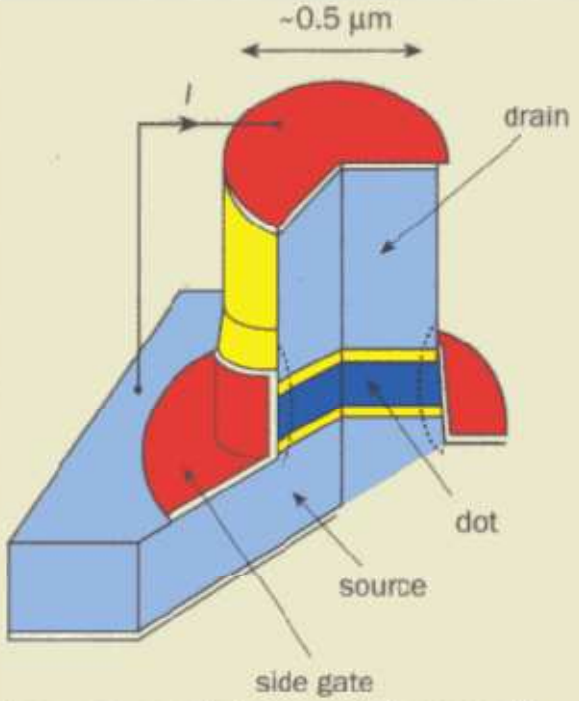

The quantum-dot structure studied at Delft and NTT in Japan is fabricated in the shape of a round pillar. The source and drain are doped semiconductor layers that conduct electricity, and are separated from the quantum dot by tunnel barriers 10 nm thick. When a negative voltage is applied to the metal side gate around the pillar, it reduces the diameter of the dot from about 500 nm to zero, causing electrons to leave the dot one at a time.

2 Artificial atoms

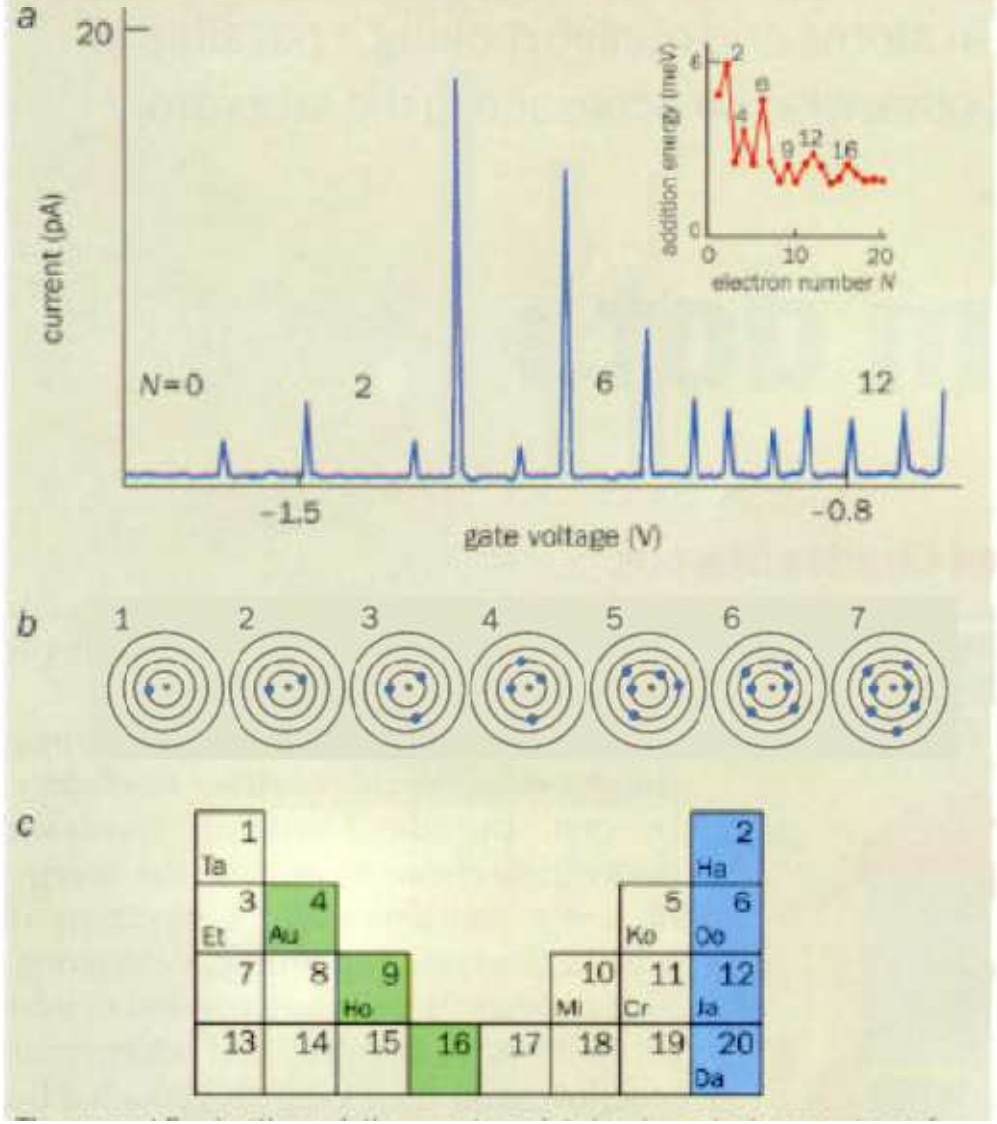

HF mean field

$$\mathcal{H} = \sum_{i=1}^{N} \left[\frac{\mathbf{p}^2}{2m} + \frac{1}{2} m\omega_0^2 r^2 \right]_i + \sum_{i>j=1}^{N} \frac{e^2}{\kappa\, r_{ij}} \ ,$$

- oscillator units: energy $\hbar\omega_0$

  length $\ell_0 = \sqrt{\dfrac{\hbar}{m\omega_0}}$

  mass m

- New Hamiltonian

$$\mathcal{H} = \sum_{i=1}^{N} \left[-\frac{1}{2}\nabla^2 + \frac{1}{2} r^2 \right]_i + R_W \sum_{i>j=1}^{N} \frac{1}{r_{ij}} \ .$$

one parameter $R_W = \dfrac{e^2/(\kappa\ell_0)}{\hbar\omega_0}$

- The HF equations in oscillator basis

$$\{\,|a\eta\rangle;\; a=1,\ldots\mathcal{N};\; \eta=\uparrow,\downarrow\,\}$$

$$\left[-\frac{1}{2}\nabla^2+\frac{1}{2}r^2\right]|a\rangle=\varepsilon_a^{(0)}|a\rangle$$

  - The HF sp states $|i\rangle=\sum_{a\eta}B_{a\eta}^{(i)}\,|a\eta\rangle\ .$

  - Up or down spins $B_{a\eta}^{(i)}=\delta_{\eta\eta_i}B_{a\eta_i}^{(i)}$

$$\varepsilon_a^{(0)}B_{a\eta_i}^{(i)}\ +\ \sum_{c=1}^{\mathcal{N}}B_{c\eta_i}^{(i)}\left[\sum_{bd=1}^{\mathcal{N}}v_{abcd}\left(\sum_{k=1}^{N}B_{b\eta_k}^{(k)}B_{d\eta_k}^{(k)}\right)-\sum_{bd=1}^{\mathcal{N}}v_{abdc}\left(\sum_{k=1}^{N}\delta_{\eta_i\eta_k}B_{b\eta_k}^{(k)}B_{d\eta_k}^{(k)}\right)\right]=\varepsilon_i B_{a\eta_i}^{(i)}\ .$$

analytical

- densities $\rho_{\mathrm{HF}}(\mathbf{r}) = \sum_{i,occ} |\langle \mathbf{r}|i\rangle|^2 = \sum_{i,occ} |\varphi_i(\mathbf{r})|^2 \,,$

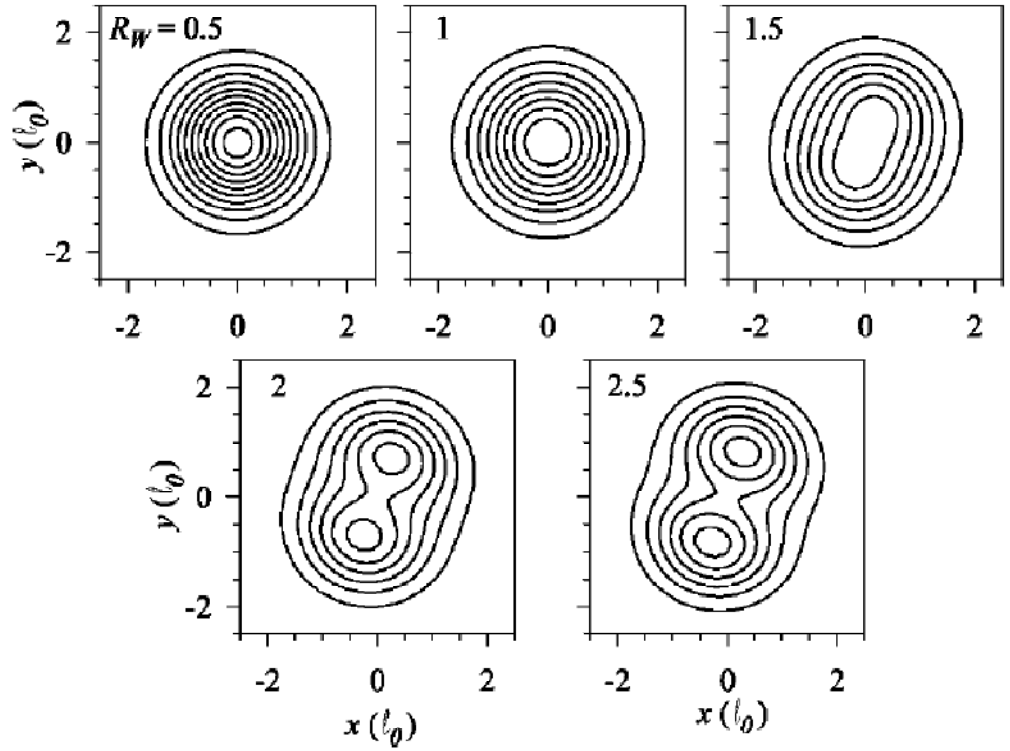

FIG. 1. HF densities for the $N=2$ quantum dot with varying R_W parameter (shown in the upper left corner of each panel). From the outermost contour line inwards each line corresponds, respectively, to a density of 0.05, 0.10, 0.15, ... , etc in units of ℓ_0^{-2}. The cutoff in the basis has been chosen $E_c \approx 10.6\, E_0$, corresponding to a basis size $\mathcal{N}=55$.

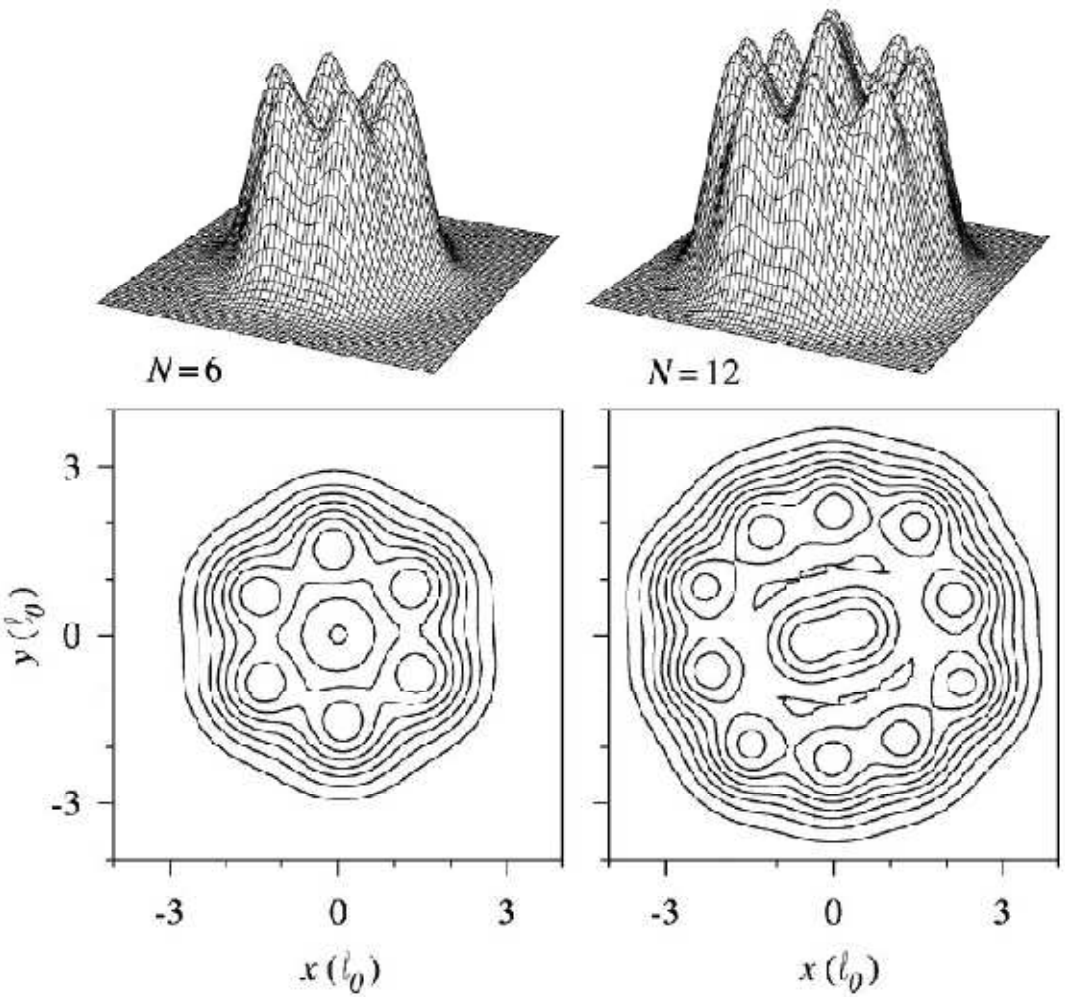

FIG. 2. Same as Fig. 1 for the $N=6$ and 12 quantum dots. For clarity the upper plots display a 3D view of the corresponding densities. The contour lines are defined as in Fig. 2 and we have used $R_W=1.89$. The basis cutoffs for $N=6$ and 12 are $E_c = 16\ E_0$ and $18\ E_0$, respectively.

- **RPA excitations**

$$O^\dagger_\lambda = \sum_{mi} \left(Y^{(\lambda)}_{mi}\, a^\dagger_m a_i - Z^{(\lambda)}_{mi}\, a^\dagger_i a_m \right) ,$$

$$|\lambda\rangle = O^\dagger_\lambda |v_{\rm RPA}\rangle \ .$$

$$\begin{pmatrix} A & B \\ B^* & A^* \end{pmatrix} \begin{pmatrix} Y^{(\lambda)} \\ Z^{(\lambda)} \end{pmatrix} = \hbar\omega_\lambda \begin{pmatrix} Y^{(\lambda)} \\ -Z^{(\lambda)} \end{pmatrix} ,$$

$$A_{mi\,nj} = \varepsilon_{mi}\,\delta_{mn}\delta_{ij} + v_{mjin} - v_{mjni}$$

$$B_{mi\,nj} = v_{mnij} - v_{mnji} \ .$$

- Matrix elements

$$v_{mjin} = \delta_{\eta_m\eta_i}\delta_{\eta_n\eta_j} \sum_{abcd=1}^{\mathcal{N}} v_{abcd}\, B^{(m)*}_{a\eta_m} B^{(j)*}_{b\eta_j} B^{(i)}_{c\eta_i} B^{(n)}_{d\eta_n} \ .$$

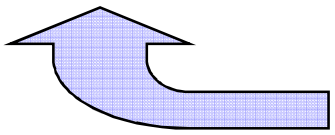

analytical

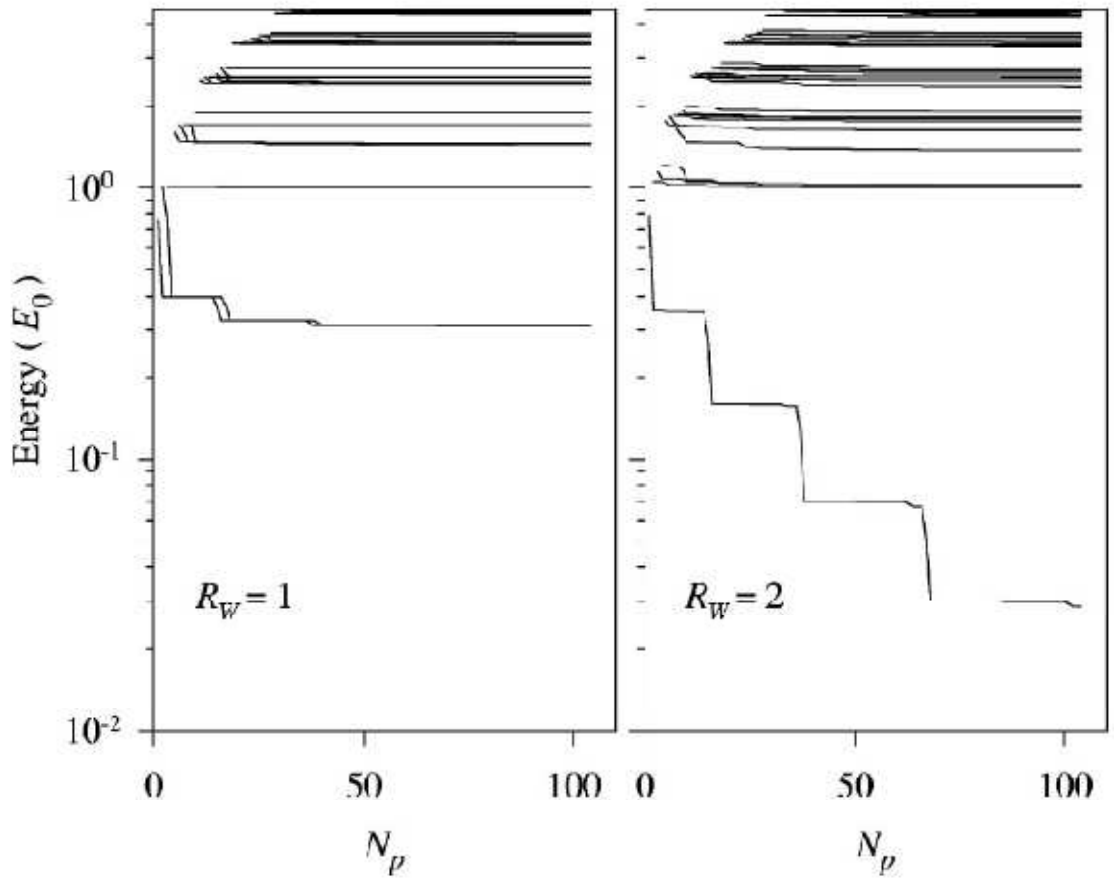

Spurious mode associated with the broken symmetry

FIG. 3. Evolution of the RPA excitation spectra with the number of particle states included. The results correspond to $N=2$ with $R_W=1$ (left) and 2 (right). The same scale has been used in both panels for a better comparison. Note that increasingly higher RPA excitations appear as N_p is increased. The same basis size and cut-off of Fig. 1 have been used.

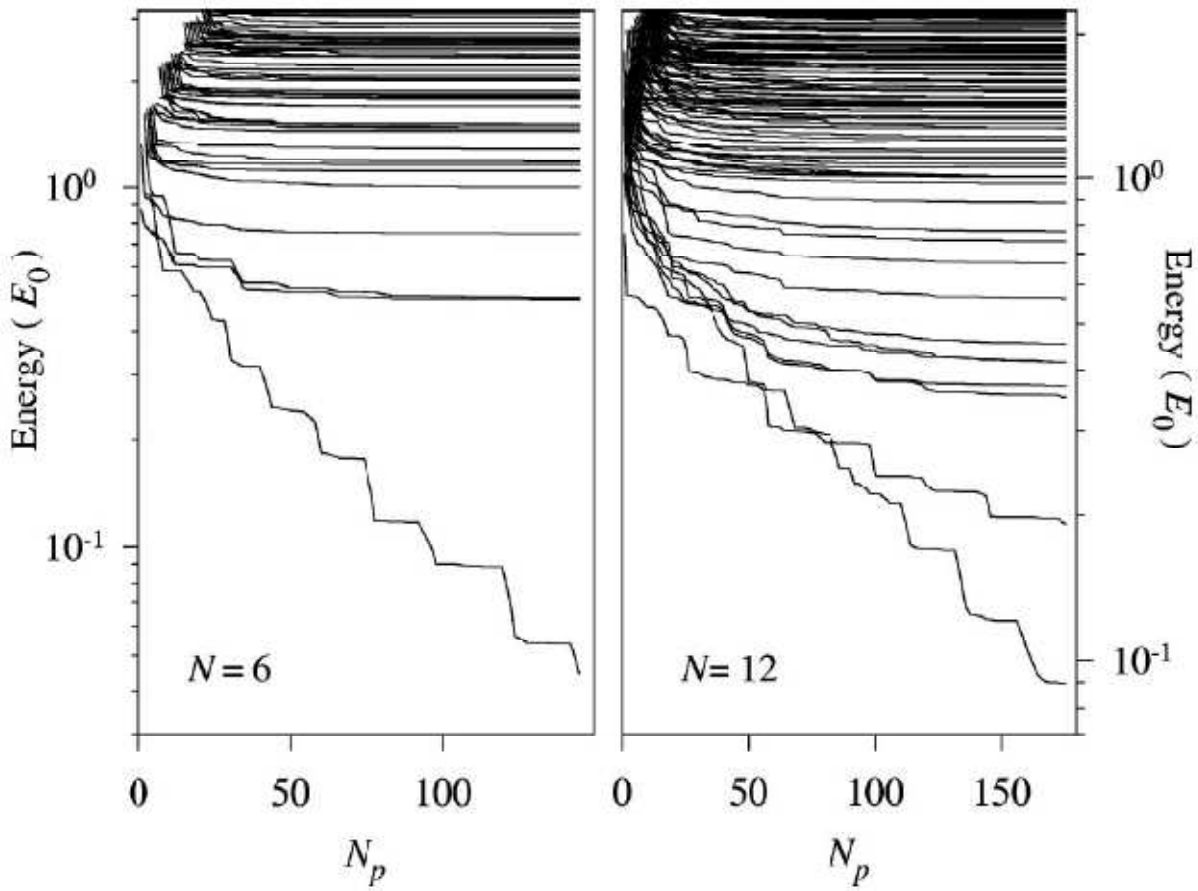

FIG. 4. Same as Fig. 3 for the $N=6$ and 12 quantum dots.

Response (strength) functions and sum rules

$$S(E) = \sum_{\lambda} \delta(E - \hbar\omega_{\lambda}) \left| \langle \lambda | W | v_{\mathrm{RPA}} \rangle \right|^2 .$$

Excitation operator

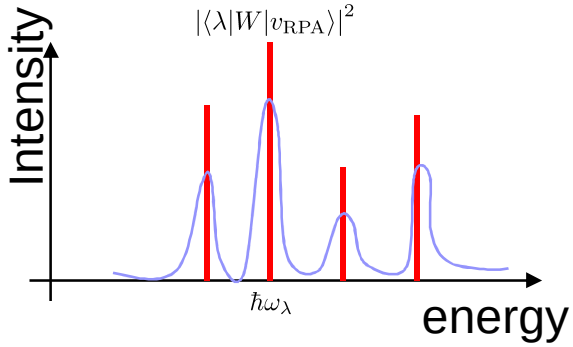

Recall that in RPA

$$\langle\lambda|W|v_{\mathrm{RPA}}\rangle = \langle v_{\mathrm{RPA}}|O_{\lambda}W|v_{\mathrm{RPA}}\rangle = \langle v_{\mathrm{RPA}}|[O_{\lambda}, W]|v_{\mathrm{RPA}}\rangle$$

$$\approx \langle v|[O_{\lambda}, W]|v\rangle = \sum_{mi} (Y^*_{mi} w_{mi} + Z^*_{mi} w_{im})$$

For comparison, in HF

$$S(E) = \sum_{mi} \delta(E - \varepsilon_{mi}) \left| \langle mi^{-1} | W | v \rangle \right|^2 .$$

$$\langle mi^{-1}|W|v\rangle = \sum_{\alpha\beta} w_{\alpha\beta} \langle v|a_i^+ a_m a_{\alpha}^+ a_{\beta}|v\rangle = w_{mi}$$

Sum rules: energy weighted moments

$$S_k \;=\; \sum_{\lambda} (\hbar\omega_\lambda)^k \;\left|\, \langle \lambda |\, W \,| \upsilon_{\mathrm{RPA}} \rangle \,\right|^2 \;\; .$$

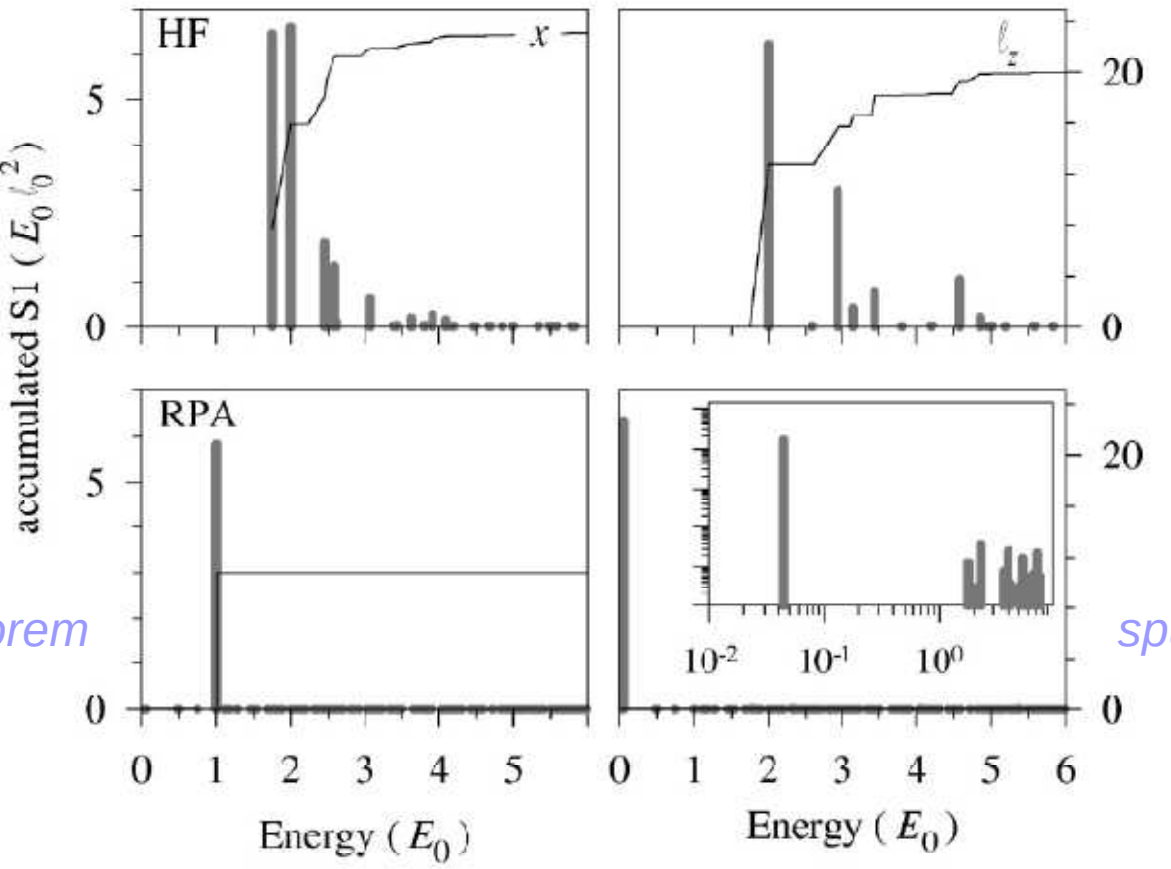

Kohn theorem

spurious mode

FIG. 5. HF and RPA excitation cross sections for the $N=6$ quantum dot. Vertical bars show in an arbitrary scale the position and height for each state while the solid line displays the accumulated contributions to the $S1$ sum rule. Left and right panels correspond to the dipole (x) and rotation (ℓ_z) operators, respectively. The inset in the bottom-right panel shows an enlarged view, using logarithmic scales, of the RPA ℓ_z cross section.

RPA ground state and its energy

- Vacuum condition $O_\lambda |v_{\rm RPA}\rangle = 0 \ , \quad \text{for all } \lambda \ .$

- Energy $E_{\rm RPA} = E_{\rm HF} - \Delta_{\rm RPA} \ .$

Correlation energy

$$\Delta_{\rm RPA} = \frac{1}{2}\left({\rm Tr} A - \sum_{\omega_\lambda > 0} \hbar\omega_\lambda \right) \ .$$

- Occupation numbers

$$\langle v_{\rm RPA}| a_m^\dagger a_m |v_{\rm RPA}\rangle = \frac{1}{2}\sum_{i\lambda} |Y_{mi}^{(\lambda)}|^2$$

$$\langle v_{\rm RPA}| a_i^\dagger a_i |v_{\rm RPA}\rangle = 1 - \frac{1}{2}\sum_{m\lambda} |Y_{mi}^{(\lambda)}|^2 \ .$$

  - Plus spurious mode contribution

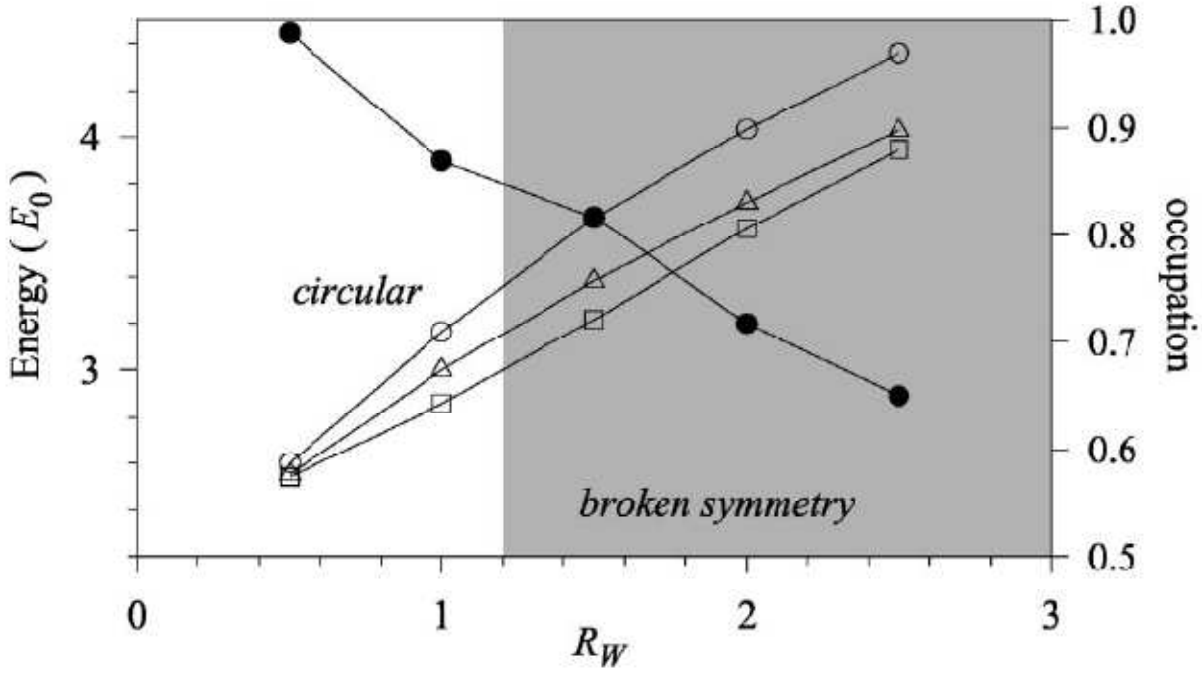

FIG. 7. Results for the two-electron dot as a function of R_W. Right scale corresponds to the occupation numbers of the HF hole state (solid symbols) while left scale indicates the ground state energies in HF (circles), RPA (squares) and exact solution (triangles). See the discussion about occupation numbers see in Sec. IV C.

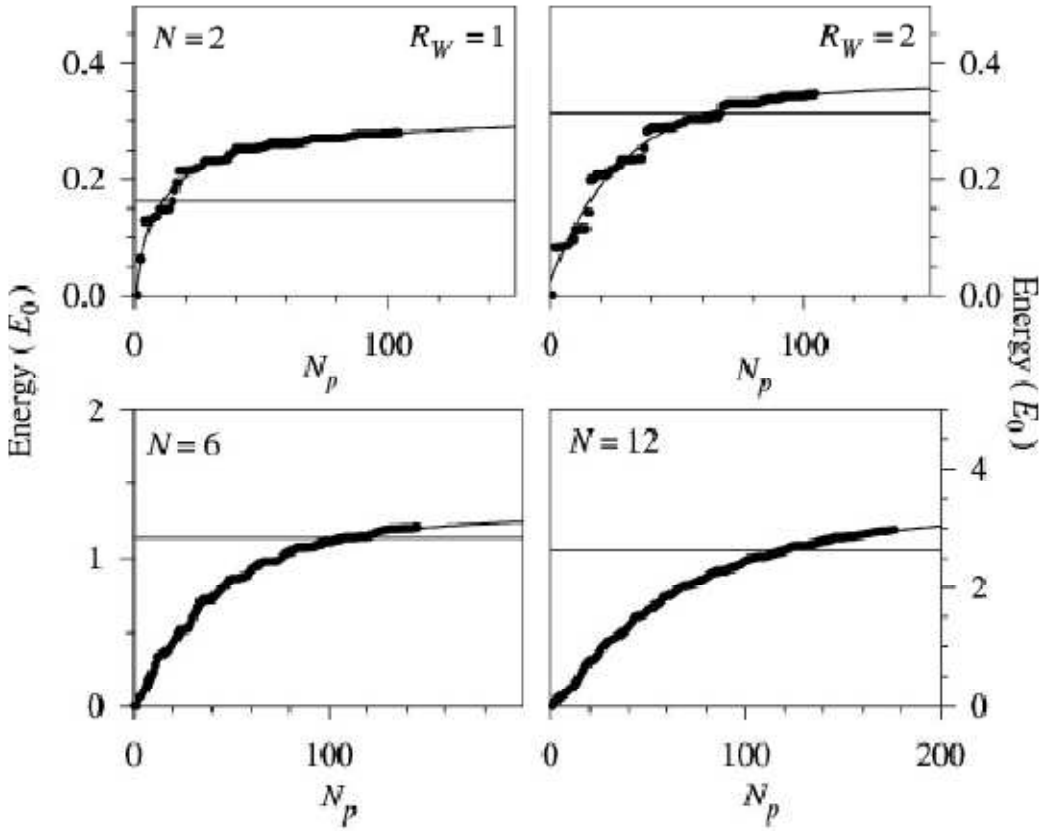

FIG. 6. Convergence with number of particle states of the RPA correction energy Δ_{RPA}. The extrapolated line as well as the exact value (horizontal line) are also shown. The exact values for $N=6$ and 12 have been taken from the Monte Carlo results of Ref. 17.

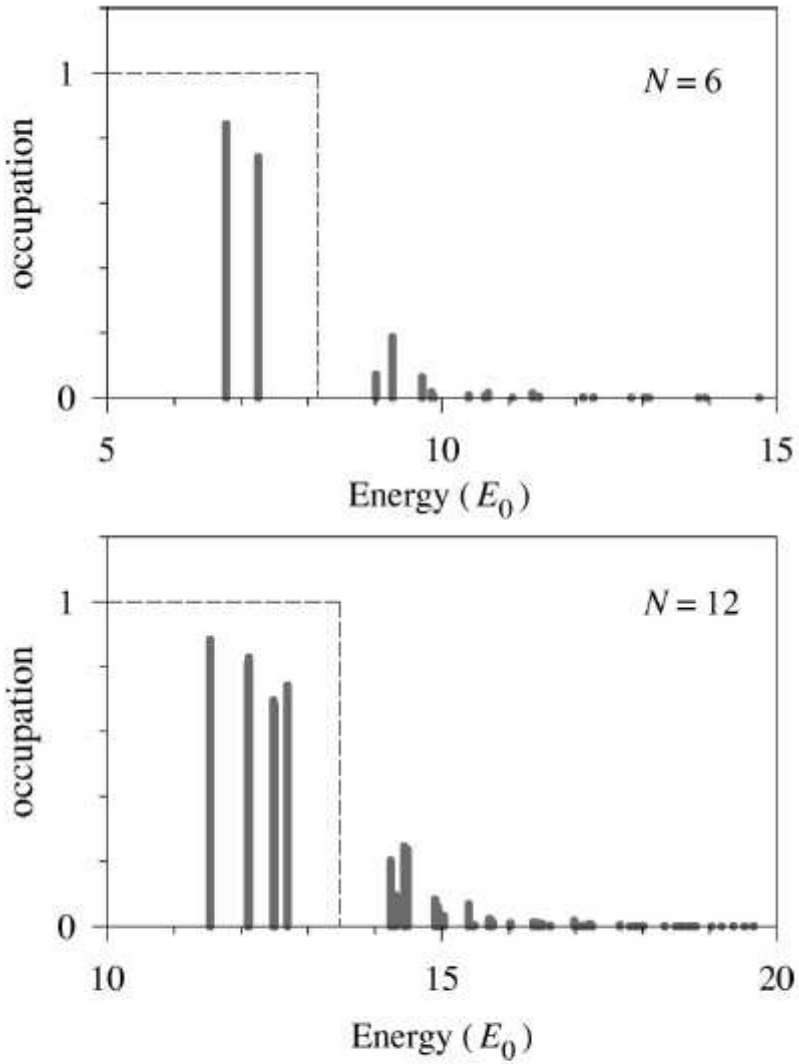

FIG. 8. Occupation numbers within RPA of the HF single-particle orbitals. The step function shown with a dashed line separates fully occupied from unoccuppied HF orbitals in the mean-field picture.

Symmetry restoration

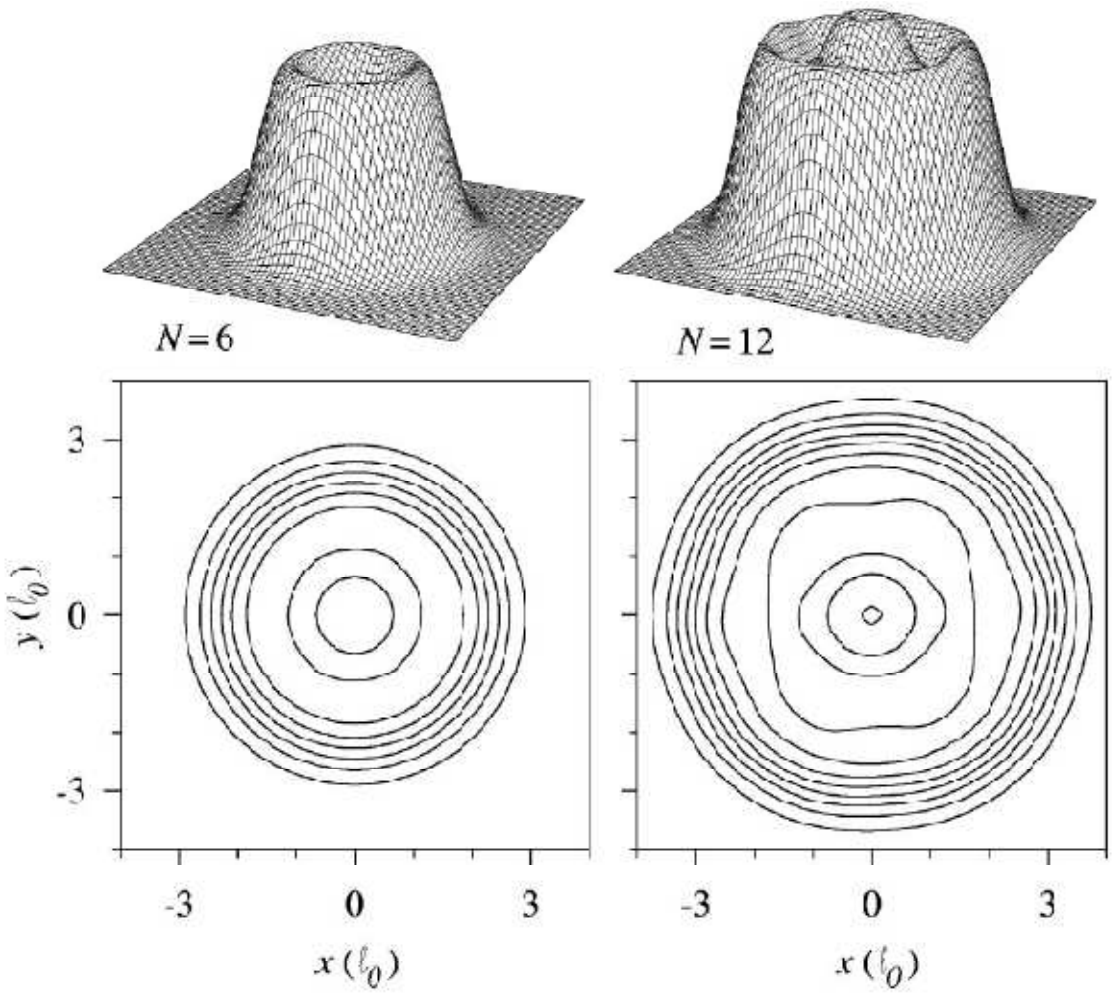

FIG. 10. RPA symmetry restoration of the HF densities displayed in Fig. 2.

Conclusions

- An application of RPA theory to quantum dots
- Coulomb interaction
- Based on the HF description
- Symmetry breaking for strong interaction
- Excited states in RPA
- Spurious modes
- Correlation energies
- Occupation numbers
- Symmetry restoration